ARTICLE

Received 00th January 20xx,
Accepted 00th January 20xx

DOI: 10.1039/x0xx00000x

www.rsc.org/

Chiral nanostructure in polymers under different deposition conditions observed by atomic force microscopy of monolayers: Poly(phenylacetylene)s as a case study

F. Freire*, E. Quiñoá and R. Riguera*

Dynamic poly(phenylacetylene)s (PPAs) adopt helical structures with different elongation or helical sense, depending on the type of pendants. Hence, a good knowledge of the parameters that define their structures becomes a key factor in the understanding of their properties and functions. Herein the techniques used for the study of the secondary structure of PPAs by atomic-force microscopy (AFM) are presented, with special attention to the methods for the preparation of monolayers, and their consequences in the quality of the AFM images. Thus, monolayers formed by drop casting, spin coating followed by crystallization or annealing, Langmuir-Blodgett and Langmuir-Schaefer methods, onto highly oriented pyrolytic graphite (HOPG) or mica are described, together with the AFM images and the resulting helical structure obtained for different PPAs. Also, some conclusions are assessed both on the adequacy of the different techniques for the formation of monolayers and on the solid supports employed to elucidate the secondary structure of different PPAs.

Introduction

Poly(phenylacetylene)s[1-9] (PPAs) are a family of dynamic helical polymers [10-16] where the helical sense,[5,17] helical scaffold[18-21] or both at the same time,[22-27] can be tuned by the action of external stimuli. This property makes these materials very interesting in fields such as sensing,[28-29] chiral separations[30] or asymmetric synthesis.[31-33]

Centro Singular de Investigación en Química Biolóxica e Materiais Moleculares (CIQUS) and Departamento de Química Orgánica, Universidade de Santiago de Compostela, 15782 Santiago de Compostela, Spain E-mail: felix.freire@usc.es, ricardo.riguera@usc.es

Félix Freire obtained his B. Sc. (2000), M. Sc. (2002) and Ph. D. (2005) degrees in Chemistry from the University of Santiago de Compostela (USC) working on determining the absolute configuration of polyfunctional compounds by NMR. During 2005-2008 he performed two postdoctoral stays at Prof. Jesús Jiménez Barbero (CSIC-Madrid) and Prof. Samuel H. Gellman (Univ. of Wisconsin-Madison) groups interested in the folding of biomolecules. Since 2009 he works at the University of Santiago as "Ramón y Cajal" researcher interested in stimuli-responsive polymers, polymer self-assembly and chiral polymer particles.

The elucidation of the secondary structure adopted by PPAs is complicated by the dynamic character of the helix of these polymers that presents variations both in sense and in chain elongation.[34]

Generally speaking, the structural determination of PPAs has been addressed mainly by the following techniques: ^{1}H-NMR[35-37] and Raman[38-42] spectroscopies, that inform on the *cis/trans* configuration of the polyenic double bonds; DSC thermograms, that are used to prove the presence of *cis-cisoidal* or *cis-transoidal* backbones (Figure 1);[43] and X-ray spectroscopy, that provides important structural parameters of the helices such as pitch, diameter, and distances between pendants within the crests.[18,20,21,44-46] Finally, CD spectra provide information on the helical sense of the polyenic backbone, while UV-Vis informs on its degree of elongation/compression.

Prof. Ricardo Riguera is full Professor in Organic Chemistry at the Universidad de Santiago de Compostela (Spain) and PI at the CIQUS Research Centre of the USC. He has authored more than two hundred papers covering Bioactive Natural Products, Medicinal Chemistry and NMR Methods for determination of Absolute Configuration. In the last few years he has concentrated on Polymeric Nanostructures for Biomedical Applications and on Stimuli Responsive Dynamic Helical Polymers.

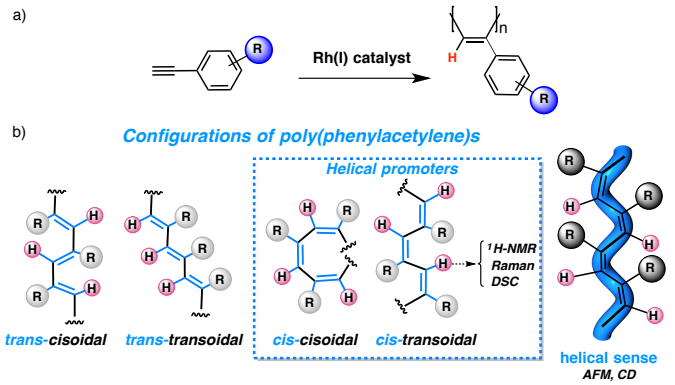

Fig. 1. a) Synthesis of PPAs. b) Possible configurations adopted by PPAs.

It is quite important to mention here that PPAs are geometrically constituted not by one, but by two coaxial helices. The internal one is formed by the polyenic skeleton, results from the positive/negative *cis-transoid* or *cis-cisoid* dihedral angle and can be studied by CD.

The additional external helix is defined by the orientation of the pendants around the axis of the backbone, and due to its peripheral position, it can be observed by AFM when the PPA is deposited on a solid support (Figure 2).

The helical senses of the internal and external helices of a PPA can be coincident or not, and therefore, the structural characterisation of these polymers is not satisfied just with CD. As a result, solid phase techniques, accounting for the external helix, have to be used (Figure 2). This is particularly important when properties related to the chirality of the surface, to the polymer or to its aggregates (e.g., recognition, catalysis, aggregation, macroscopical chirality…) are sought.

As indicated, atomic force microscopy (AFM) allows visualizing the secondary structure of a helical PPA, measuring the packing angle and pitch and determining the helical sense.[47-48] Unfortunately application of this technique is not straightforward. The preparation of the sample becomes a critical task because only well-ordered self-assembled monolayers give AFM images with resolution high enough to distinguish the details of the external helix.[34, 47, 48]

Emilio Quiñoá got his Ph.D. degree in Chemistry (University of Santiago de Compostela, USC) working in Marine Natural Products. After postdoctoral research at the University of California, Santa Cruz (UCSC), he became Associate Professor and later Professor at USC. He has co-authored more than one hundred scientific publications, a number of textbooks, patent applications, and has received several research awards. After working for more than a decade in NMR Methods for the Assignment of Absolute Configuration, in 2010 he joined the Center for Research in Biological Chemistry and Molecular Materials (CIQUS) at USC, where his current research interests are focused on the study of Dynamic Helical Polymers and their Applications in Nanotechnology.

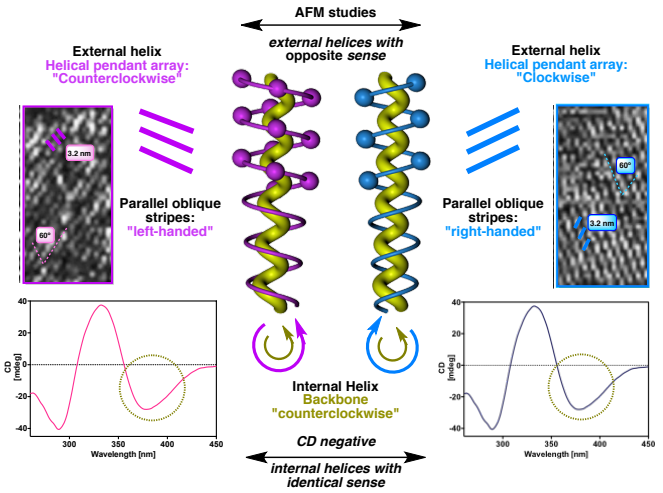

Fig. 2 Examples of different helical structures adopted by PPAs where the two coaxial helices rotate in the same or opposite sense.

In addition, the monolayer must be deposited on an appropriate substrate, because the interactions between the solid support and the polymer can affect, not only to the intermolecular assembly of the polymer chains, but also to its helical conformation.[47, 48] During the last decade several procedures have been developed to create well-ordered monolayers of PPAs and good quality AFM images.

In this feature article, we summarize those results, paying special attention to the secondary structures obtained for several PPAS by AFM of monolayers prepared by drop casting, spin coating, Langmuir-Blodgett and Langmuir Schaefer methods.

Researchers should also be aware that, although AFM allows the direct observation of helical structures, artifacts that complicate structural analysis are sometimes present in the AFM images. In order to avoid misinterpretations, the combination of AFM information with XRD analysis has been shown to be useful in some cases.[34, 47]

Drop casting

In a pioneering work, Yashima and co-workers tried to solve the structure of a helical PPA bearing bulky pendants by casting a solution of the polymer on two different substrates, highly oriented pyrolytic graphite (HOPG) and mica.[49] More precisely, they studied a phenylacetylene copolymer [i.e., poly($\mathbf{1}_x$-*co*-$\mathbf{2}_{1-x}$)], composed by two pendants: an achiral C_{60}-bound and an optically active amine (*i.e.*, (*R*)-[(1-phenylethyl)carbamoyl]oxy). This copolymer was deposited by drop casting both on freshly cleaved mica and on HOPG, and the morphologies of the resulting assemblies were studied by AFM (Figures 3a and 3b). The AFM images on mica (cast from THF) showed isolated particles originating from aggregation of the C_{60} groups in clusters as a result of the repulsion between the hydrophobic C_{60} units and the hydrophilic mica substrate. In contrast, deposition of the copolymer on HOPG instead of mica led to images showing extended and individual copolymer chains together with some isolated particles (Figure 3b). These results indicate that the attractive force between

the pendant fullerenes and the solid substrate plays a critical role in the morphology of the C_{60}-based polymers and suggest that the interplay between the hydrophobic/hydrophilic nature of the support and the pendants of the polymer can be used to select the formation of a certain class of suprastructure.[49]

Similar studies were carried out on low- and high-molecular-weight poly(4-carboxyphenylacetylene)s (poly-**3**), their salts with (*R*)-(+)-1-(1-naphthyl)ethylamine [(R)-**4**, Figure 3c] and on the corresponding carboxyamides (poly-**5**; Figure 3c). These polymers were deposited by drop casting on mica, and AFM showed the presence of isolated chains with a helical structure. Although the helical sense could be determined, the quality of the images was not good enough to provide reliable values for the pitch distance and packing angle.[50]

In a related example, poly-**6** and poly-**7**, bearing as pendant groups different chiral forms of a bulky ruthenium complex, were prepared (Figure 3d), and the supramolecular structures formed by their deposition on mica investigated.[51] The polymers adsorbed on mica clearly showed isolated strands, and visualization of the right- and left-handed helices was possible by AFM.[51]

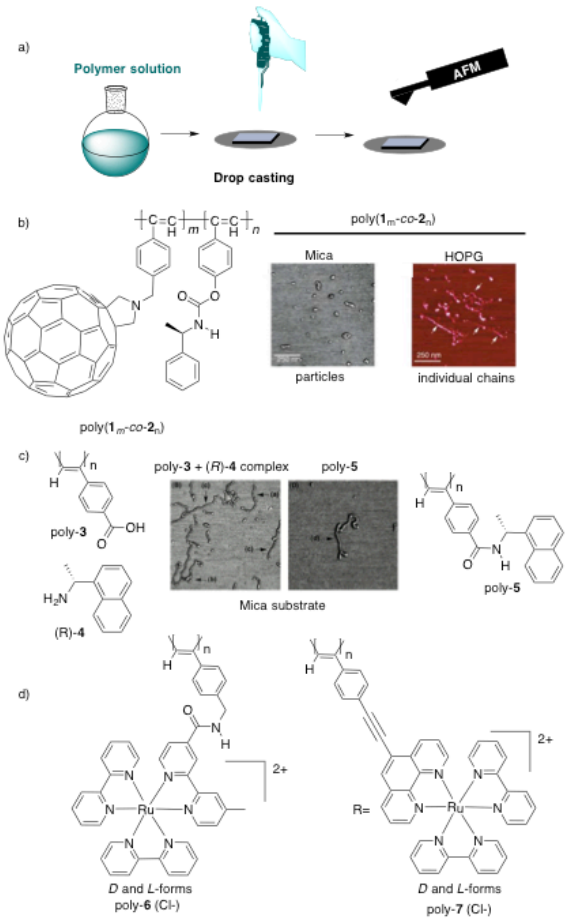

Fig. 3 a) Schematic representation of the drop casting procedure for the preparation of PPA monolayers. b) Structure and AFM images of poly(**1**$_m$-*co*-**2**$_n$) drop casted onto mica and HOPG. Reproduced from Ref. 49 with permission from the Wiley. c) Structure and AFM images of poly-**5** and the poly-**3**/(*R*)-**4** complex drop casted onto mica substrate. Single molecules, toroidal structures and superhelices are observed (see also Ref. 47). Reproduced from Ref. 50 with permission from the American Chemical Society. d) Structure of *D*- and *L*-forms of poly-**6** (Cl^-) and poly-**7** (Cl^-).

Spin coating and solvent vapour exposure

In a second approach, Yashima reasoned that the introduction of long alkyl chains as pendants of the PPA backbone, should promote the self-assembly of PPA chains through the interdigitation of the long chain groups.[52-54] The sample for AFM was prepared by spin coating a dilute solution of the PPA onto the solid substrate (mica or HOPG) and kept under solvent atmosphere overnight in order to favour the self-assembly of the polymer chains.[53] Using this procedure, Yashima *et al.* obtained the helical structure of poly-(*D*)-**8** and poly-(*L*)-**8**, bearing *D*- and *L*-alanine bonded to a long alkyl chain (i.e., $C_{10}H_{21}$, Figure 4a).[53] In those conditions, the polymers formed well-ordered 2D-crystals thanks to the strong and epitaxial adsorption of the alkyl chains of the pendant on the graphite lattice (Figures 4c-e). AFM images of poly-(*L*)-**8** indicated the presence of a helical structure with a helical pitch of 2.34 nm and a packing angle of 40°, where the pendant groups describe a 11/5 (external) *M* helical structure, with two residues per turn (Figure 4c).[53] For its part, the internal polyenic backbone adopts a *cis-transoidal* configuration and describes a right-handed (*P*) helical sense with a pitch of 2.3 nm. Thus, in these compounds, the pendant groups describe a left-handed helical array (AFM, Figure 4c), whereas the polyene backbone rotates describing a right-handed helical structure (CD with a blue line, Figure 4b).

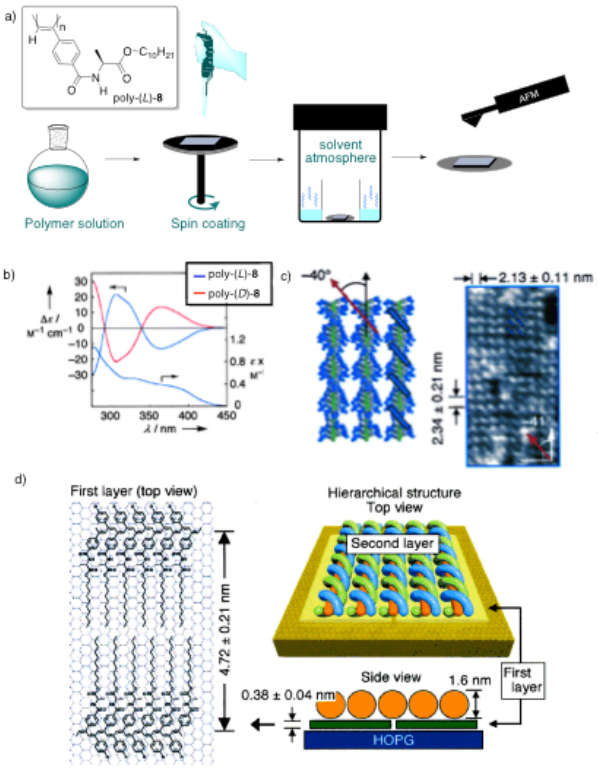

Fig. 4 a) Structure of poly-(*L*)-**8** and schematic representation of the spin coating/solvent atmosphere procedure for the formation of PPA monolayers. b) CD spectra of poly-(*L*)-**8** and poly-(*D*)-**8** in benzene. c) AFM images of 2D self-assembled poly-(*L*)-**8** on HOPG and helical structures proposed by AFM and XRD analyses. d) Schematic representation of the hierarchical structure of the self-assembled poly-(*L*)-**8** on HOPG. Reproduced from Ref. 53 with permission from the Wiley-VCH.

Moreover, the dynamic behaviour of the PPAs in the solid state was demonstrated by using this protocol. So, poly-(*D*)-**8** could invert its helical structure depending on the polarity of the solvent used for the formation of the 2D-crystals onto the AFM substrate (HOPG, Figure 5).[54] These results were in agreement with the effects observed by CD in solution. Thus, a first positive Cotton effect was observed when the polymer was dissolved in benzene (right-handed pendant helical array determined by AFM, *cis-transoidal* backbone). However, the polymer showed a first negative Cotton effect when was dissolved in more polar solvents such as THF or $CHCl_3$ (left-handed pendant helical array determined by AFM, *cis-transoidal* backbone, Figure 5).[54]

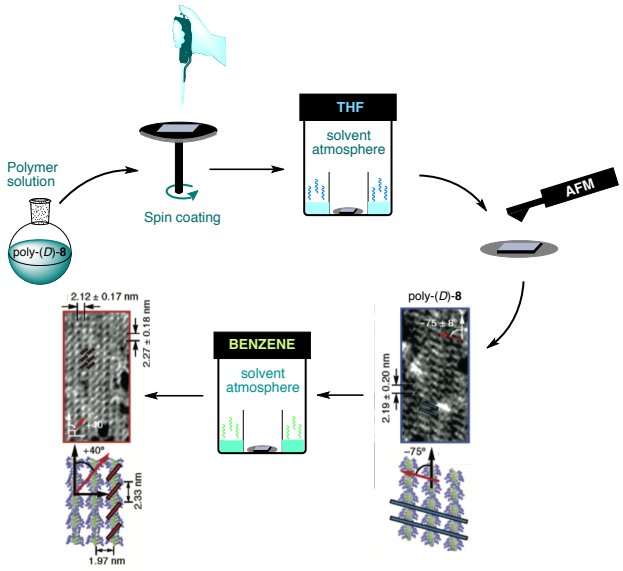

Fig. 5 Graphical representation of the spin coating/solvent atmosphere (THF) protocol. It produces a well ordered monolayer of poly-(*D*)-**8** followed by a helix inversion induced in the solid state by exposure to solvent atmosphere (benzene). Reproduced from Ref. 54 with permission from the American Chemical Society.

Next, the same group studied the helical structure of an achiral PPA by using the same technique. They chose, as model polymer, a PPA bearing α-aminoisobutyric acid (Aib) *n*-decyl esters as achiral pendants (poly-**9**, Figure 6a).[55] Interestingly, AFM studies revealed the presence of mixtures of left- and right-handed helical structures within the same 2D-crystal (Figures 6b-c). The high quality of the 2D crystal allowed obtaining different helical parameters in addition to the helical sense, such as the helical pitch or molecular packing (*P* helix: 2.01 nm helical pitch, +43° packing angle; M helix: 2.05 nm helical pitch, -45° packing angle; Figure 6c). During the analysis of the AFM images obtained for different 2D-crystals, the authors could observe a different packing pattern between homochiral helices (same helical sense), and heterochiral helices (opposite helical sense) in the 2D-crystals. While homochiral helices were packed parallel to each other and without showing any shifting among them (Figure 6c, red bars only), heterochiral helices (Figure 6c, red and blue bars) were packed in a parallel fashion but with a shift of one-third helical pitch relative to each other with respect to the main-chain axis (Figure 6c, thin white solid lines).

During these studies, the authors could also corroborate the presence of rarely occurring reversals. These structural features make possible that helices with opposite helical sense can coexist within the same polymer chain (Figure 6c).

The combination of the information obtained from AFM, and other structural techniques such as X-ray, NMR and Raman, allowed the authors to elucidate the secondary structure of poly-**9**, a 11/5 helical structure with two residues per turn, where the polyene backbone adopts a *cis-transoidal* configuration. In this type of helical structure, the helices described by the polyene backbone and by the pendant groups show opposite senses.[55]

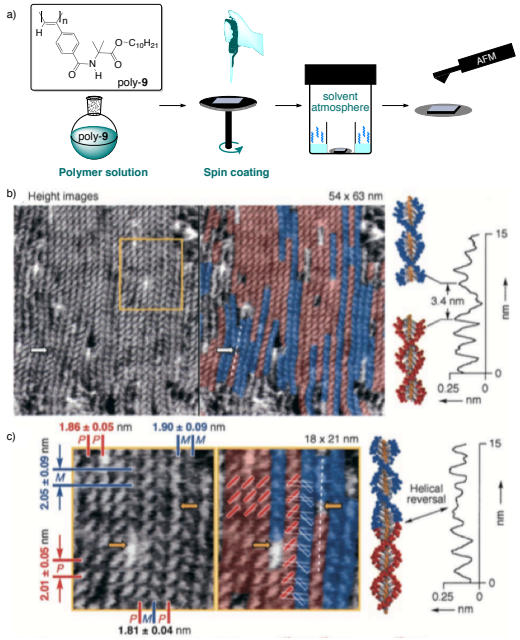

Fig. 6 a) Structure of poly-**9** and schematic representation of the spin coating/solvent atmosphere procedure for the formation of PPA monolayers. b) AFM height images of 2D self-assembled poly-**9** cast on HOPG showing the presence of right- (red) and left-handed (blue) helices within the same 2D crystal. c) AFM image of a well-ordered monolayer of poly-**9** highlighting the presence of helical reversals. Reproduced from Ref. 55 with permission from the Wiley.

In another interesting work, Yashima *et al.* describe the visualisation in the solid state of a chiral amplification phenomena occurring in a copolymer that behaves as helically racemic in solution. To demonstrate this effect, the authors prepared a series of copolymers [poly-(*L*)-**8**-*co*-**9**] composed by a combination of a chiral monomer bearing (*L*)-alanine decyl

ester as pendants, and an achiral monomer bearing Aib decyl ester (Figure 7a).[56] CD experiments showed that while the homopolymer [poly-(*L*)-**8**] presents in benzene a strong CD signature, the introduction within the polymer chain of just a 5% of the achiral monomer results in the complete lost of the helical chirality, and the resulting copolymer [poly-(*L*)-**8**-*co*-**9**] shows a null CD (Figure 7b).

Nevertheless, when the 2D-crystals prepared by spin coating of the copolymer solution were deposited on HOPG and exposed to a benzene atmosphere, AFM revealed the presence of well-ordered *M* helices, packed in a parallel fashion just like in the homochiral poly-(*L*)-**8** polymer[56] (Figures 7c-d).

AFM showed that poly-(*L*)-$\mathbf{8}_x$-co-$\mathbf{9}_{1-x}$ copolymers adopt a preferred 11/5 helix (two residues per turn), with the pendant groups describing a left-handed helical array. In solution, the negative CD indicates that the polyene backbone rotates describing a right-handed helical structure. Therefore in these copolymers the internal and external helices present opposite senses.

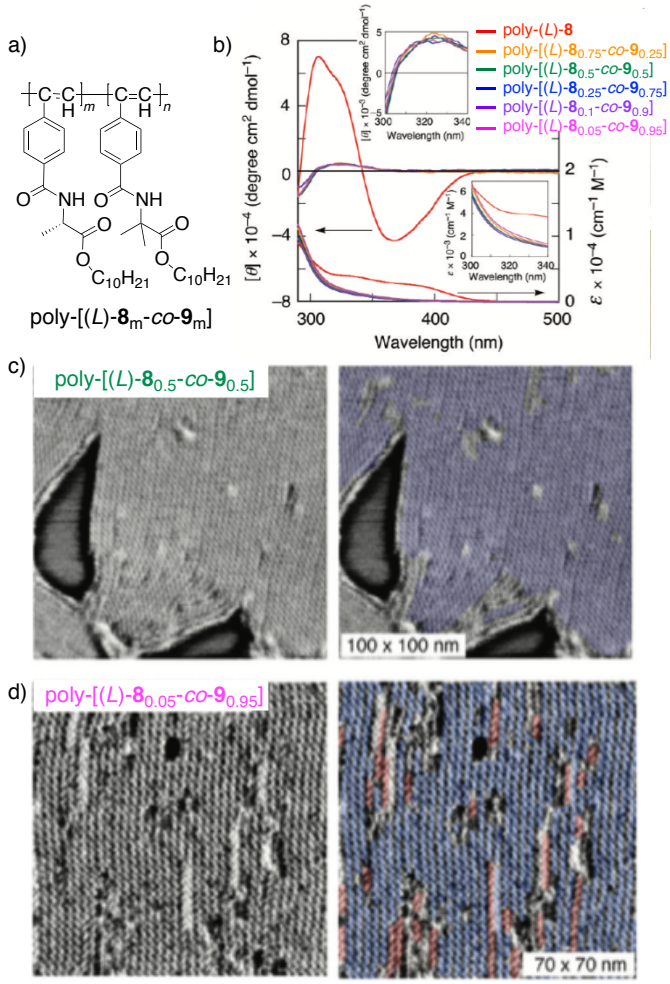

Fig. 7 a) Structure of poly-[(*L*)-$\mathbf{8}_m$-*co*-$\mathbf{9}_m$]. b) CD spectra showing the absence in solution of the Sergeants and Soldiers effect for the copolymer series poly-[(*L*)-$\mathbf{8}_m$-*co*-$\mathbf{9}_m$]. AFM images of 2D self-assembled (c) poly-[(*L*)-$\mathbf{8}_{0.5}$-*co*-$\mathbf{9}_{0.5}$] and (d) poly-[(*L*)-$\mathbf{8}_{0.05}$-*co*-$\mathbf{9}_{0.95}$] on HOPG indicating the effectiveness of the Sergeants and Soldiers effect in the solid state. Reproduced from Ref. 56 with permission from the American Chemical Society.

Apart from that example of activation of the Sergeants and Soldiers effect in the solid state, the same group also studied the chiral amplification based on "majority rules" using copolymers [poly-(*L*)-$\mathbf{8}_x$-*co*-(*D*)-$\mathbf{8}_{1-x}$]. It was observed that the copolymer containing a very low excess of (*L*)-Ala produced 2D-crystals with a 89% excess of *M* helical sense.[57]

Using this protocol, we succeeded in the preparation of good quality 2D-crystals from several PPAs bearing short pendants, showing that the presence of long alkyl chains is not always necessary for the self-assembly of PPAs.

As a first approach,[58] we applied the spin coating/solvent exposure procedure to the helically racemic poly-(*R*)-**10**, deposited on HOPG, but we did not observe the presence of 2D-crystals, probably due to the intrinsic high dynamic behaviour of poly-(*R*)-**10** (Figure 8).

This dynamism is related to the pendant of poly-(*R*)-**10**, constituted by the anilide of (*R*)-α-methoxy-α-phenylacetic acid (MPA, Figure 8). This pendant exists as a 1:1 equilibrium between two conformers (*ap*: carbonyl and methoxy groups antiperiplanar oriented; and *sp*: carbonyl and methoxy groups in synperiplanar orientation).[58] Each one has the bulkiest group (i.e., aryl ring) in a different orientation producing a different interaction with the surroundings and favouring a different helical sense in the backbone. The 1:1 conformational composition of the pendants is therefore transmitted to a 1:1 equilibrium of *P*/*M* helical senses.

However, well-ordered monolayers of poly-(*R*)-**10** were obtained when the 1:1 *P*/*M* equilibrium is shifted to the right- or left-handed sense by chiral amplification with mono- or divalent metal ions.[58-60]

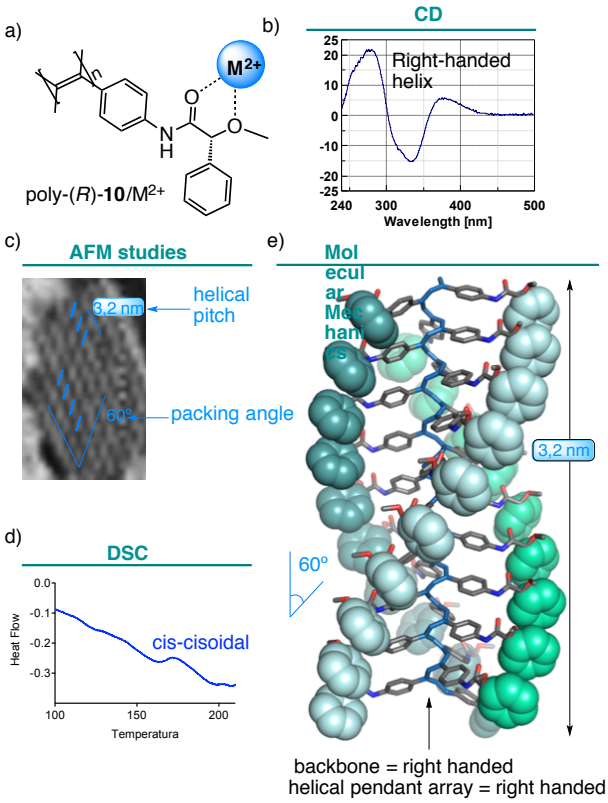

Fig. 8 a) Structure of poly-(*R*)-**10**/M^{2+} HPMC. Structural techniques employed to solve the tridimensional structure of poly-(*R*)-**10**/M^{2+}: (b) CD, (c) AFM, (d) DSC and (e) MM calculations.

Thus, when a dilute solution of the helical polymer-metal complex (HPMC) was spin coated onto HOPG and left under a THF atmosphere overnight, good quality monolayers were formed.[58] AFM showed well-ordered 2D-crystals, revealing the helical pitch (3.2 nm), the packing angle (60°), and the helical sense described by the pendant array (left-handed in poly-(*R*)-**10**/M^+ complexes and right-handed in poly-(*R*)-**10**/M^{2+} complexes, Figure 8).

In another work we showed that the left-handed helix of the monovalent metal complex [i.e., poly-(*R*)-**10**/M^+] can be selectively inverted to right-handed in solution by cleavage of the cation-π interaction with a small amount of a polar cosolvent. Spin-coating/solvent exposure procedure served us to demonstrate that both the left- and the right-handed helices are maintained in the 2-D crystal (Figure 9).[61, 62]

These data, in combination with the information obtained from other structural techniques (NMR, Raman, DSC, CD), allowed us to completely elucidate the secondary structure of these helical polymers metal complexes (Figure 8).[58, 61]

Interestingly, poly-(*R*)-**10**, adopts a *cis-cisoidal* configuration at the polyene, resulting in a helical structure that has three residues per turn (3/1), and rotates (internal helix) in the same sense than the external helix formed by the pendants. This result differs from the opposite sense found by Yashima *et al.*[52-55] in their *cis-transoidal* PPAs.

Application of this spin coating-solvent exposure technique to other HPMCs with short pendants, gave also high-quality 2D-crystals and allowed the evaluation of the helical parameters.[63-64]

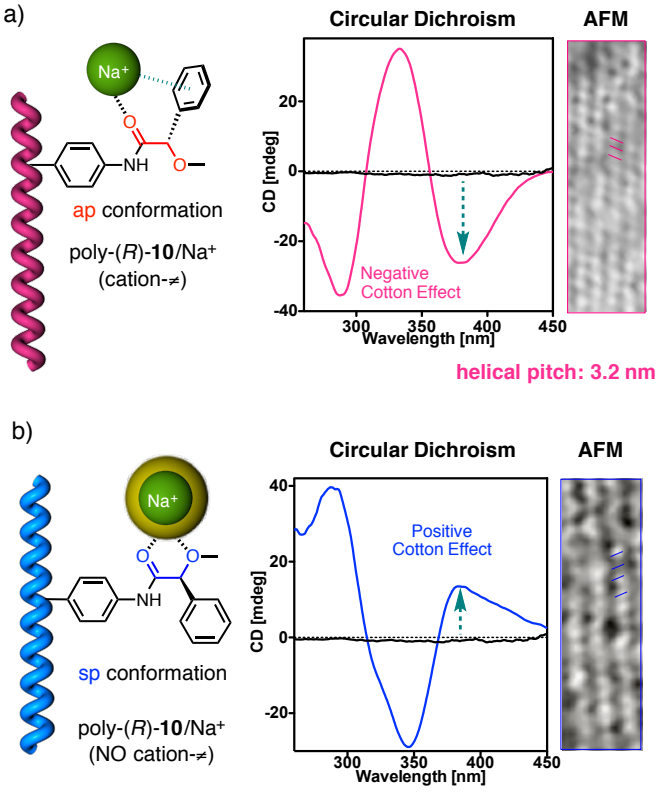

Fig. 9 CD spectra and AFM images of the (a) left- and (b) right-handed helical structures induced in the poly-(*R*)-**10**/Na^+ complex due to the (a) presence and (b) absence of cation-π interactions. Reproduced from Ref. 61 with permission from the Royal Society of Chemistry.

During our studies with PPAs with short pendant groups, we described a dynamic polymer, poly-(*R*)-**11**, bearing the anilide of (*R*)-α-methoxy-α-trifluoromethyl-α-phenylacetic acid (MTPA) as pendant group (Figure 10). Both the elasticity (stretched/compressed) and helical sense (clockwise/anticlockwise) of this PPA can be selectively tuned by the donor and polar character of the solvent.[65-66]

The basis for this behaviour lies on the presence in the pendant of two independent tuneable bonds: (O=)C–C(–O) and (H-)N–C(=O). Thus, while the (O=)C–C(–O) bond shifts between two different conformations by the polarity of the solvent (*ap*: carbonyl and methoxy groups *antiperiplanar* oriented, *sp*: carbonyl and methoxy groups *synperiplanar* oriented; Figure 10a), the (H–)N–C(=O) bond remains unaffected by changes on the polarity but adopts two different conformations depending on the donor character of the solvent (*cis*: amide in *cis* and *trans*: amide in *trans*; Figure 10a). In this way, changes on the polarity of the solvent affect exclusively the helical sense of the PPA (visualized by CD), but changes on the donor character of the solvent affect both the elongation of the polymer chain and the helical sense (visualized as UV-Vis bathochromic shift and CD inversion respectively; Figure 10b).

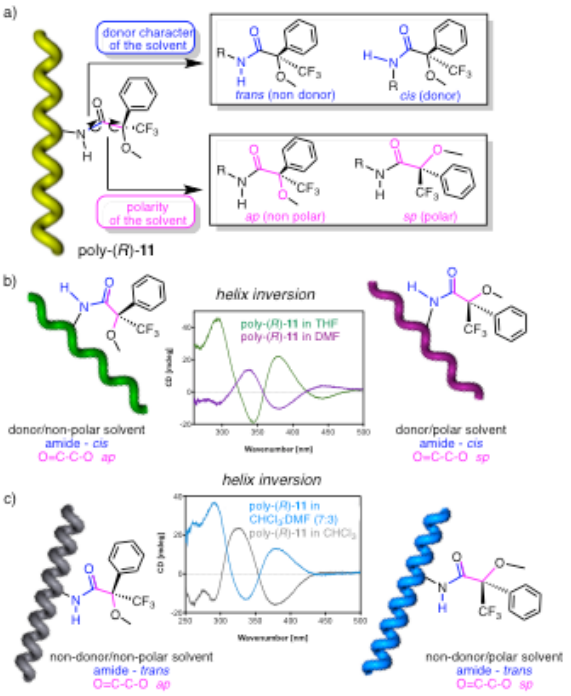

Fig. 10 a) Conformational equilibrium of the (H–)N–C(=O)(amide) and (O=)C–C(–O) bonds of poly-(*R*)-**11**. b) Conformational changes in an extended helical scaffold (*cis*-amide) due to the polarity of the solvent. (c) Conformational changes in a compressed helical structure (*trans*-amide) due to the polarity of the solvent. Reproduced from Ref. 65 with permission from the Royal Society of Chemistry.

In order to know if this structural tuning of the helix can be transferred from solution to solid state, we prepared well-ordered self-assembled 2D-crystals of poly-(*R*)-**11** by spin

coating in different solvent conditions and transferred them onto a HOPG surface.[65]

Thus, 10 μL of a $CHCl_3$ (non-donor/low-polar) solution of poly-(*R*)-**11** were spin coated onto HOPG, and the sample placed under $CHCl_3$ vapours overnight. Similarly, 10 μL of a THF (donor/low-polar) solution of poly-(*R*)-**11** were spin coated and maintained under a THF atmosphere overnight.

AFM studies revealed that the 2D-crystal of poly-(R)-**11** prepared in $CHCl_3$ present a parallel packing of chains with a right-handed pendant disposition (clockwise), 50° periodic oblique stripes and a 3.0 nm helical pitch (Figure 11).

On the other hand, the 2D-crystal prepared in THF showed the polymer chains packed also in a parallel fashion but forming a right-handed (clockwise) pendant disposition with the periodic oblique stripes at 40° and a helical pitch of 3.9 nm (Figure 12).

Thus, the two different scaffolds, one compressed ($CHCl_3$) and the other stretched (THF) are clearly observed in the 2D crystals by AFM. In both cases, the helical array described by the pendant (external) is right-handed while the CD spectra show opposite Cotton effects at the polyene region (negative CD in $CHCl_3$ and positive CD in THF).

In $CHCl_3$, poly-(*R*)-**11** presents a *cis-cisoidal* polyene backbone, describing a helix with three residues per turn (compressed), where both the internal polyenic helix and the external helix described by the pendants rotate in the same direction (Figure 11). On the other hand, poly-(*R*)-**11** dissolved in THF shows a more stretched *cis-transoidal* helical structure, where the internal and external helices rotate in opposite ways (Figure 12).

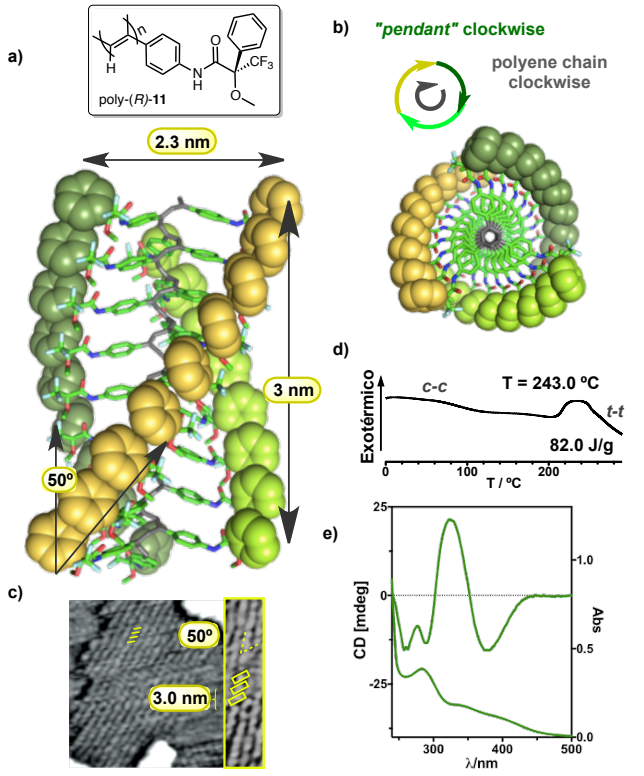

Fig. 11 Helical structure of poly-(*R*)-**11** in $CHCl_3$ obtained from molecular mechanics calculations (MMFF94) and AFM studies: (a) side view and (b) top view. (c) AFM studies of poly-(*R*)-**11** in $CHCl_3$. (d) DSC trace of poly-(*R*)-**11** (film) prepared in $CHCl_3$. (e) CD and UV-Vis studies of poly-(*R*)-**11** in $CHCl_3$. Reproduced from Ref. 65 with permission from the Royal Society of Chemistry.

The robustness of the spin coating followed by solvent exposure procedure for preparation of well-ordered 2D-crystals has been further demonstrated by its application to numerous helical polymers and double helices. Its success allowed the determination by AFM of numerous secondary structures and the measurement of the relevant helical parameters (helical sense, pitch, packing angle).[3, 34, 47, 67-70]

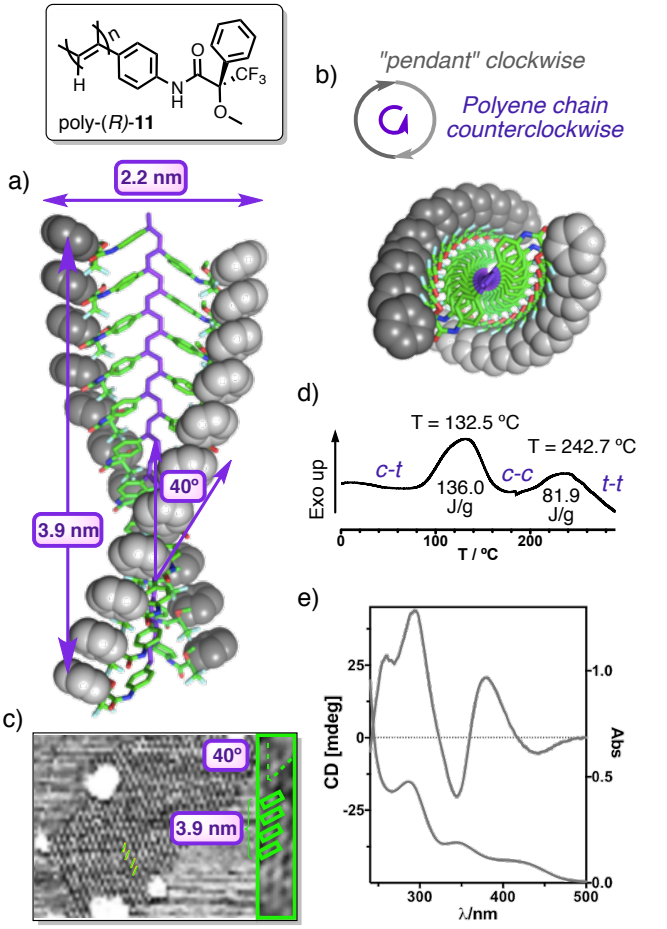

Fig. 12 Helical structure of poly-(*R*)-**11** in THF obtained from molecular mechanics calculations (MMFF94) and AFM studies: (a) side view and (b) top view. (c) AFM studies of poly-(*R*)-**11** in THF. (d) DSC trace of poly-(*R*)-**11** (film) prepared in THF. (e) CD and UV-Vis studies of poly-(*R*)-**11** in THF. Reproduced from Ref. 65 with permission from the Royal Society of Chemistry.

Spin coating and thermal annealing

In a parallel research, Percec and co-workers developed a similar protocol to produce 2D crystals either on HOPG or on mica that allowed visualizing the self-organization of individual dendronized PPAs by AFM. It is based on spin coating, but instead of promoting crystallization by exposure of the monolayer to solvents, in Percec's procedure, the monolayer is submitted to thermal annealing. To perform their studies, they prepared a library of dendronized PPAs (from poly-**12** to poly-**26**), with long alkyl tails, essential to promote the self-assembly (Figures 13 and 14).[71-73]

Thus, *cis-transolidal* poly(carbazolylacetylene) poly-**14** (Figure 13), after spin casting on graphite accompanied by thermal annealing at 100ºC, was visualized by AFM as individual chains.[71] The detailed AFM study[73] of another of those dendronized PPAs (i.e., poly-**21**) deposited on HOPG (Figure 15) showed individual macromolecules as oblate cylindrical objects. Their orientation in the first layer, the one directly adsorbed on the HOPG, reflected the underlying lattice symmetry due to the adsorption of the long alkyl tails. Another consequence of epitaxy was that at the HOPG interface, the PPA backbone adopted a more extended conformation than in the hexagonal columnar phase found in bulk.

Although no values for helical pitches or packing angles were reported in this work, the presence of well-ordered monolayers and the AFM images indicate the high potential of this procedure for obtaining that kind of information.

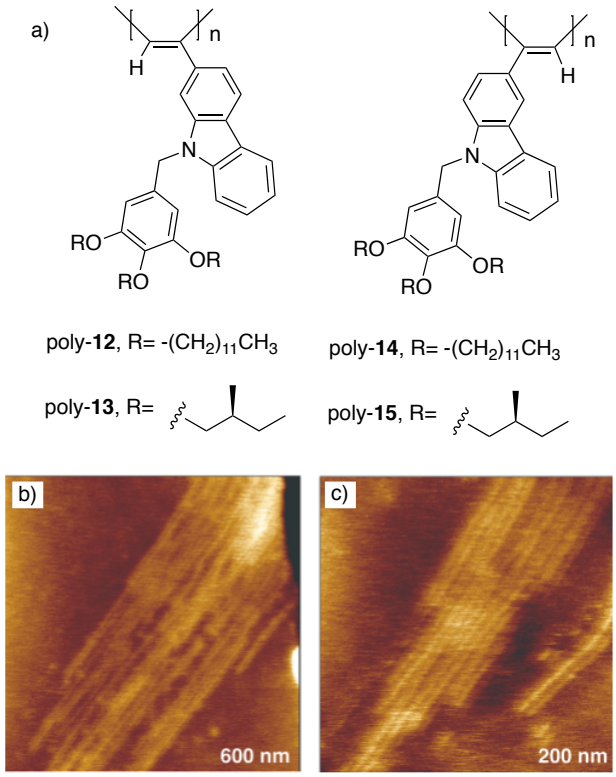

Fig. 13 a) Structures of poly-**12**, poly-**13**, poly-**14** and poly-**15**. b) and c) AFM images of poly-**14** on graphite after annealing at 100 °C. Reproduced from Ref. 71 with permission from Wiley-VCH.

Langmuir-Blodgett

The previous methods for preparation of monolayers rely on the evaporation of a solution of the polymer on a solid support, the monolayer being formed in the air/solid interface. In those conditions, the interactions of the polymer with the support and the character and evaporation rate of the solvent are critical factors. In contrast, the Langmuir-Blodgett (LB) method prepares monolayers in an air/water interphase,[74, 75] and therefore, the hydrophilic/hydrophobic character of the polymer and the solid support play a very important role.

Tang and co-workers studied the formation of monolayers by this technique, using PPAs with hydrophobic backbone and bearing hydrophilic pendants such as amino acid residues. Namely, they prepared poly-(*L*)-**27**,[76, 77] containing the benzamide of (*L*)-alanine methyl ester as pendant, and poly-(*L*)-**28**[78-81] containing the benzamide of (*L*)-valine methyl ester, whose amphiphilic character was expected to promote self-assembly at the air water interphase (Figure 16).

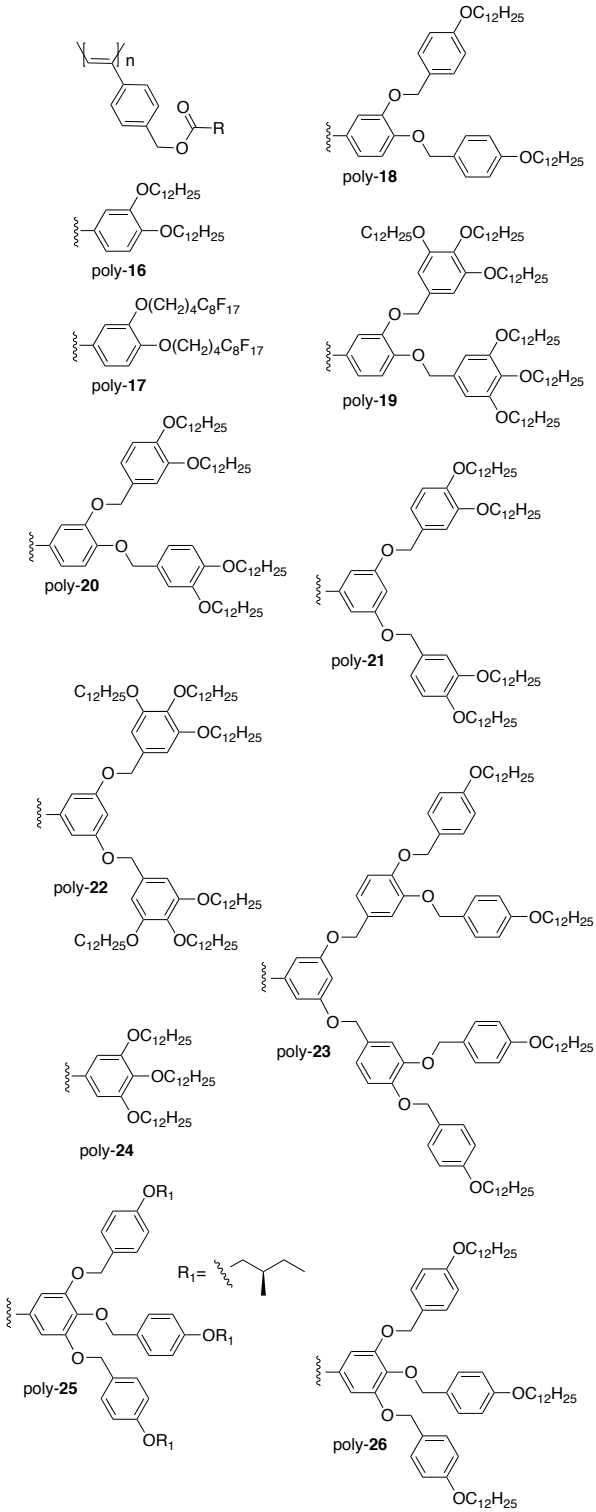

Fig. 14 Structures of dendronized PPAs (from poly-**16** to poly-**26**). Reproduced from Ref. 72 with permission from Wiley.

To perform these studies they smoothly spread a dilute THF solution of the PPA onto the water surface. Next, by compressing the water surface, the surface pressure of the polymers gradually increases until it reaches a point where a compact polymer monolayer is formed (20 mN/m for poly-(*L*)-**27**[76] and 40 mN/m for poly-(*L*)-**28**).[78] The process can be visualized through the isotherms that exhibit two regions: the low surface pressure region —lower than 15 mN/m), where the surface pressure region gradually increases with compression—, and the high surface pressure region —higher than 15 mN/m, where the surface pressure abruptly increases with compression—. The limiting area for poly-(*L*)-**27**[76] is 0.68 nm^2 and 0.38 $nm^2$for poly-(*L*)-**28.**[78]

The monolayer formed in this way is then transferred to the surface of freshly cleaved mica, with its hydrophilic side facing the solid support and the hydrophobic part exposed to the air. AFM showed the presence of well-ordered 2D crystals although the quality of the images was not enough to obtain the helical sense, pitch or packing angle of either poly-(*L*)-**27** or poly-(*L*)-**28** (Figure 16).

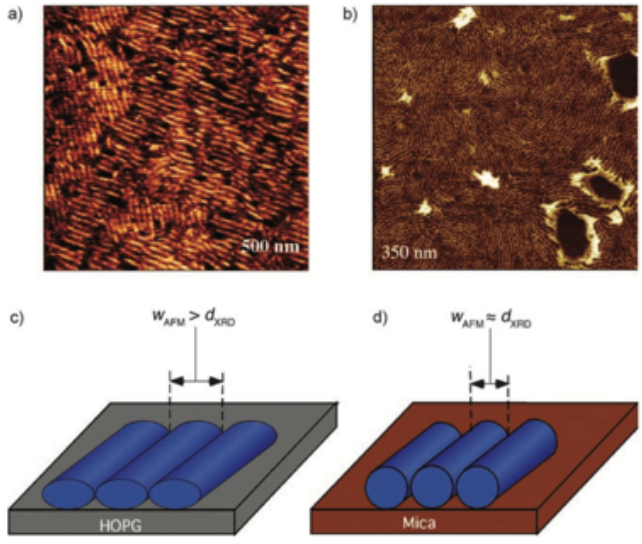

Fig. 15 AFM visualizations of poly-**21** on (a) HOPG and (b) mica. Illustrations of cylindrical PPAs on (c) HOPG and (d) mica. The oblate shape on HOPG is due to epitaxial adsorption of the alkyl tails on the graphite underlayer. Reproduced from Ref 72 Copyright 2006 Wiley-VCH.

Langmuir-Schaefer

As shown before, LB works well with polymers with amphiphilic character where the hydrophilic part is used to fix the monolayer onto the hydrophilic mica. Nevertheless, the literature shows that the best AFM images for this class of polymers are usually obtained when the monolayer is formed on HOPG. This substrate is more hydrophobic than mica, showing a better interaction with the PPAs and favouring the monolayer formation. Unfortunately, these hydrophobic properties of HOPG, so adequate for the polymer, are incompatible with its use in LB because the substrate has to be extracted from the water layer.

In order to prepare well ordered monolayers of our PPAs bearing short pendants, on HOPG, we used the Langmuir-Schaefer (LS) approach,[82] a modification of LB where the monolayer is exfoliated from the interphase instead of extracted (LB), allowing its transfer to HOPG.[83]

In this way, good monolayers of the highly dynamic and helically racemic poly-(*R*)-**8** were obtained and its secondary structure, previously unavailable by the other techniques, [83] was fully determined.

To perform these studies, a dilute solution of poly-(*R*)-**8** in $CHCl_3$ was spread droplet by droplet (200 μL) onto a pool of water. Then, smooth evaporation of the $CHCl_3$ took place (5 min approximately), followed by a gradual compression of the polymer surface until a compact monolayer of poly-(*R*)-**8** was formed.

The surface pressure/molecular area (π–A) isotherm of a poly-(*R*)-**8** layer prepared at 0.5 mN exhibited two distinct regions with very different slopes: at compressions lower than 0.3 mN m^{-1}, the surface region increased gradually with compression, while at compressions higher than 0.3 mN m^{-1}, the monolayer surface increased rapidly with compression. The limiting area for poly-(*R*)-**8** was 0.15 nm^2. The monolayer of poly-(*R*)-**8** prepared in this way was transferred from the air/water interphase to a newly cleaved HOPG by exfoliation. AFM images show well-ordered monolayers, similar to those obtained for 2D crystals by spin coating/solvent exposure, with uniform fields composed by either left-handed or right-handed helical chains. No fields of mixed senses (Figure 17) were found, indicating that selective homochiral packing was in operation.

Interestingly, this packing differs from to the one reported for the achiral poly-**9** (Figure 6), where the two helical senses coexist within a single 2D-crystal.[55]

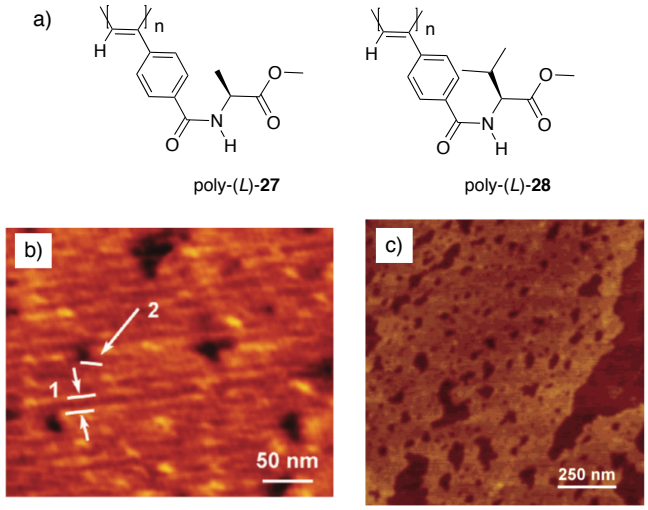

Fig. 16 a) Structure of poly-(*L*)-**27** and poly-(*L*)-**28**. AFM images of (b) poly-(*L*)-**27** and (c) poly-(*L*)-**28** monolayers obtained by Langmuir-Blodgett. Reproduced from Ref. 76 and 78 with permission from the American Chemical Society.

The high quality of these monolayers gave images that allowed determining not only the helical sense of the pendant array, but also the helical pitch (3.2 nm) and the packing angle (±60°) in the different fields.

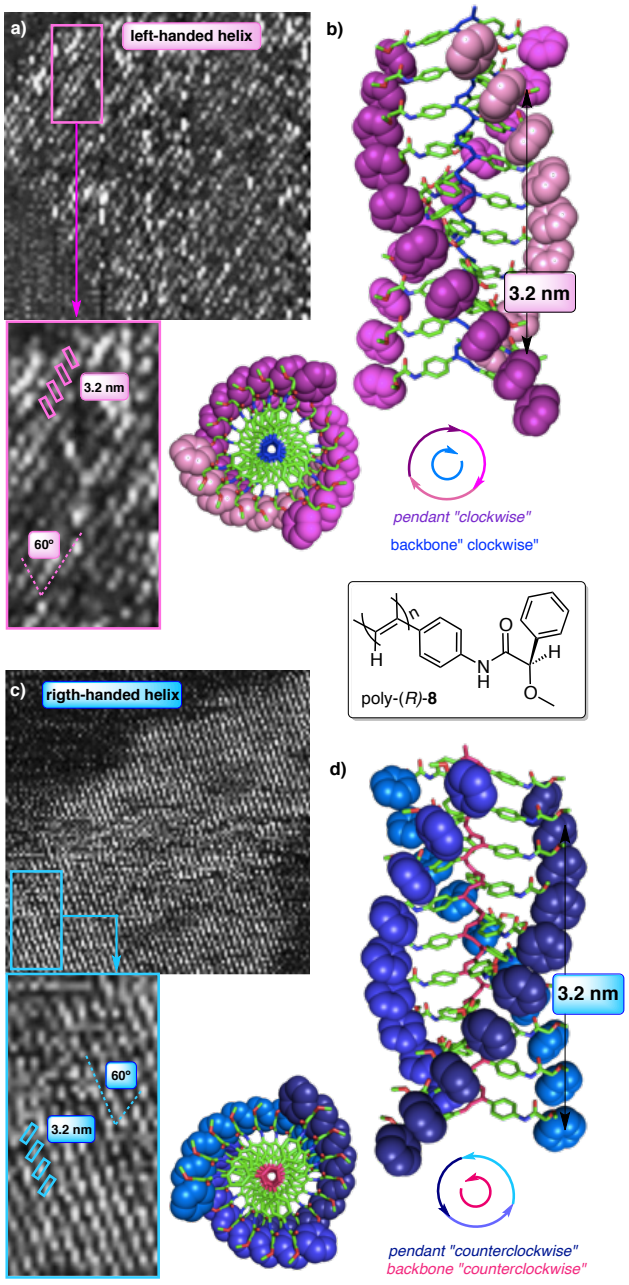

Fig. 17 a) AFM image of a well ordered monolayer of poly-(*R*)-**8** prepared by Langmuir-Schaefer showing the presence of a left-handed helical structure . b) Left-handed helical structure of poly-(*R*)-**8** obtained from molecular mechanics calculations (MMFF94) and AFM studies. c) AFM image of a well ordered monolayer of poly-(*R*)-**8** repared by Langmuir-Schaefer showing the presence of a right-handed helical structure. d) Right-handed helical structure of poly-(*R*)-**8** obtained from molecular mechanics calculations (MMFF94) and AFM studies. Reproduced from Ref. 83 with permission from the Royal Society of Chemistry.

These values are coincident with those of the polymer complexed with monovalent or divalent metal ions. They indicate that poly-(*R*)-**8** adopts a helical structure with 3 residues per turn (hydrogen bonds between the n^{th} and $(n+3)^{th}$ units), and a *cis-cisoidal* polyene backbone, where the helices described by the polyene and by the pendants rotate in the same direction (Figure 17). Interestingly, AFM showed, in addition to single chains, the presence of separate left- and right-handed oriented superhelices.[84-90]

More recently we applied the LS method to the study of some *meta* substituted PPAs: *m*-poly-(*R*)-**8**, bearing the *meta*-anilide of (*R*)-α-methoxy-α-phenylacetic acid (MPA), and *m*-poly-(*R*)-**29**, that incorporates the *meta*-benzamide of phenylglycine methyl ester (PGME) as pendant.[91]

These PPAs present equilibria between two helices with different elongation. AFM images of the 2D-crystals obtained by LS showed also two different domains specific for each helix (Figures 18 and 19) in the 2D-crystals.

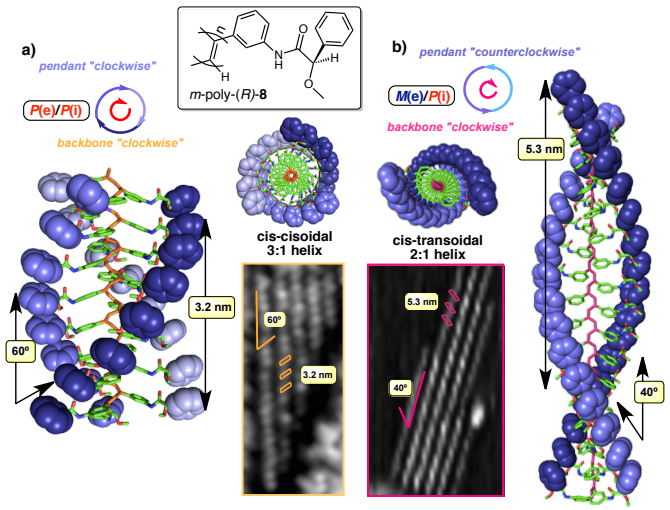

Fig. 18 AFM images of well-ordered monolayers of *m*-poly-(*R*)-**8** prepared by Langmuir-Schaefer showing the presence of two helices: a) one compressed and another b) more stretched

Thus, *m*-poly-(*R*)-**8** exists in solution as equilibrium between a compressed *cis-cisoidal* helix, with three residues per turn (helical pitch: 3.2 nm, packing angle: 60°) and a more stretched *cis-transoidal* helical structure that has 2 residues per turn (helical pitch: 5.3 nm, packing angle: 40°, Figure 18). The internal helical senses of the two forms are the same (i.e., right-handed in both cases), while the helices described by the pendants are opposite (right-handed for the compressed structure and left-handed for the stretched one, Figure 18).

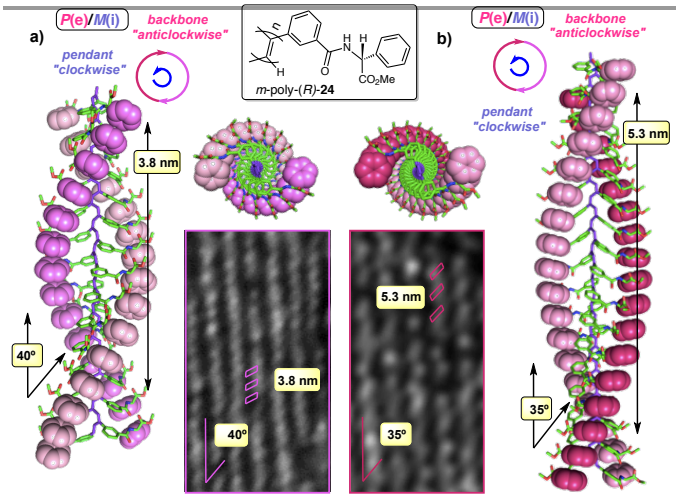

Fig. 19 AFM images of well-ordered monolayers of *m*-poly-(*R)*-**29** prepared by Langmuir-Schaefer showing the presence of two helices: a) one compressed and b) another more stretched.

For its part, *m*-poly-(*R*)-**29** is composed by two stretched *cis-transoidal* helices (one being more stretched than the other) in equilibrium. Both are *cis-transoidal* with 2 residues per turn, 3.8 nm helical pitch and 60° packing angle in the least stretched form, and 5.3 and 35° respectively in the most stretched one. In *m*-poly-(*R*)-**29**, the helical senses of the internal helices are the same (left-handed in both forms), but opposite to the sense described by the pendants (right-handed in both cases, Figure 19).

Conclusions

The secondary structure of helical poly(phenylacetylene)s is complicated not only by their dynamism, that leads to variations in sense and chain elongation, but also by the existence of two coaxial helices whose helical sense can be coincident or not: an internal one formed by the polyenic skeleton (observed by CD), and an external helix defined by the orientation of the pendants around the axis of the backbone (observed by AFM).

As the internal helix is located deeply inside the polymer, it is the external one and the substituents placed there what determines the shape and interactions between chains and with any other molecule. In this context, all applications devised for PPAs related to recognition, aggregation, chirality, catalysis, etc., depend on the secondary structure observable in the solid state.

Unfortunately, only when the polymer forms well-ordered self-assembled monolayers, AFM can yield images with resolution enough to visualize the pitch, packing angle and helical sense of the external helix. This fact renders the preparation of the monolayer a critical point.

In fact, the literature suggests that HOPG is the best AFM substrate to form well-ordered monolayers of lipophilic PPAs. Mica, that is more hydrophilic, can be a useful alternative if hydrophilic pendant groups are present and HOPG does not provide good results.

In this review we describe the results obtained using the most important techniques for preparation of monolayers based on drop casting, spin coating followed by crystallization or annealing, and the Langmuir-Blodgett and Langmuir-Schaefer methods. During this analysis we also describe the secondary structures obtained for PPAs by AFM studies, indicating the solid supports employed in the different procedures and their adequacy to every method and polymer.

Considering together all the information gathered from the literature and our own experience, some conclusions could be formulated that may facilitate the selection of the most adequate method and solid support for monolayer formation in future works.

Thus, regarding the formation of the monolayer, it seems that spin coating is very useful to obtain well ordered self-assembled monolayers from PPAs bearing pendants with long alkyl chains. Any of its two variations, crystallization and annealing, work well with those substrates, although the solvent exposure procedure apparently produces the best results. In this case, the amount of solvent used to create the solvent atmosphere and the time employed to favour the 2D-crystal formation are the parameters that have to be controlled to avoid dissolution of the crystal or the formation of amorphous aggregates.

The robustness of spin coating followed by solvent exposure allowed its successful application also to PPAs bearing short pendants. For this family of polymers, the preparation of well ordered monolayers by the Langmuir-Schaefer procedure seems to be useful too, yielding good results even for a polymer where the spin coating procedure failed [i.e., poly-(*R*)-**8**].

The fact that the monolayer is formed at the air/water interface renders the Langmuir-Schaefer procedure less convenient for PPAs with hydrophobic pendants or bearing long alkyl chains. On the other hand, drop casting and Langmuir-Blodgett protocols did not provide good results in the formation of monolayers from PPAs, indicating that they are not very useful to elucidate the secondary structure of these polymers.

Acknowledgements

This work was supported by grants from MEC (CTQ2014-61470-EXP, CTQ2015-70519-P), ERDF and Xunta de Galicia (GRC2014/040).

References

1 E. Yashima and K. Maeda, *Macromolecules*, 2008, **41**, 3.
2 J. G. Rudick and V. Percec, *Acc. Chem. Res*., 2008, **41**, 1641.
3 E. Yashima, K. Maeda and Y. Furusho, *Acc. Chem. Res.*, **2008**, 41, 1166.
4 B. M. Rosen, C. J. Wilson, D. A. Wilson, M. Peterca, M. R. Iman and V. Percec, *Chem. Rev.*, 2009, **109**, 6275.
5 E. Yashima, K. Maeda, H. Iida, Y. Furusho and K. Nagai, *Chem. Rev.*, 2009, **109**, 6102.
6 W. -S. Li and T. Aida, *Chem. Rev*., 2009, **109**, 6047.
7 J. Liu, J. W. Y. Lam and B. Z. Tang, *Chem. Rev*., 2009, **109**, 5799.
8 F. Freire, J. M. Seco, E. Quiñoá and R. Riguera, *Adv. Polym. Sci.*, 2013, **262**, 123.
9 J. Rudick, *Adv. Polym. Sci.,* 2013, **262**, 345–362.
10 T. Nakano and Y. Okamoto, *Chem. Rev*., 2001, **101**, 4013.
11 J. J. L. M. Cornelissen, A. E. Rowan, R. J. M. Nolte and N. A. J. M. Sommerdijkand, *Chem. Rev*., 2001, **101**, 4039.
12 D. J. Hill, M. J. Mio, R. B. Prince, T. S. Hughes and J. S. Moore, *Chem. Rev*., 2001, **101**, 3893.
13 M. Sugimone and Y. Ito, *Adv. Polym. Sci.,* 2004, **171**, 77.
14 J. W. Y. Lam and B. Z. Tang*, Acc. Chem. Res*., 2005, **38**, 745.
15 E. Yashima and K. Maeda, in *Foldamers: Structure, Properties, and Applications*, ed. S. Hecht and I. Huc, Wiley-VCH, Weinheim, 2007, pp. 331.
16 R. J. M. Nolte and A. E. Rowan, *Polym. Chem*., 2011, **2**, 33.
17 Y. Hu, R. Liu, F. Sanda and T. Masuda, *Polym. J.*, 2007, **40**, 143.
18 V. Percec, M. Peterca, J. G. Rudick, E. Aqad, M. R. Imam and P. A. Heiney, *Chem.–Eur. J.,* 2007, **13**, 9572.
19 V. Percec, J. G. Rudick, M. Peterca, M. Wagner, M. Obata, C. M. Mitchell, W.-D. Cho, V. S. K. Balagurusamy and P. A. Heiney, *J. Am. Chem. Soc.*, 2005, **127**, 15257.
20 V. Percec, E. Aqad, M. Peterca, J. G. Rudick, L. Lemon, J. C. Ronda, B. B. De, P. A. Heiney and E. W. Meijer*, J. Am. Chem. Soc.*, 2006, **128**, 16365.
21 V. Percec, J. G. Rudick, M. Peterca, E. Aqad, M. R. Imam and P. A. Heiney, *J. Polym. Sci., Part A: Polym. Chem.*, 2007, **45**, 4974.

22 E. Yashima, K. Maeda and O. Sato, *J. Am. Chem. Soc*., 2001, **123**, 8159.
23 K. Maeda, N. Kamiya and E. Yashima, *Chem.–Eur. J.*, 2004, **10**, 4000.
24 H. C. Zhao, F. Sanda and T. Masuda*, J. Polym. Sci., Part A: Polym. Chem*., 2005, **43**, 5168.
25 H. C. Zhao, F. Sanda and T. Masuda, *Macromol. Chem. Phys*., 2005, **206**, 1653.
26 F. Sanda, K. Terada and T. Masuda, *Macromolecules*, 2005, **38**, 8149
27 K. Maeda, H. Mochizuki, M. Watanabe and E. Yashima, *J. Am. Chem. Soc*., 2006, **128**, 7639.
28 E. Anger, H. Iida, T. Yamaguchi, K. Hayashi, D. Kumano, D. Crassous, N. Vanthuyne, C. Rousselc and E. Yashima, *Polym. Chem*., 2014, **5**, 4909.
29 H. Iida, M. Miki, S. Iwahana and E. Yashima, *Chem.–Eur. J.*, 2014, **20**, 4257.
30 K. Shimomura, T. Ikai, S. Kanoh, E. Yashima and K. Maeda, *Nat. Chem*., 2014, **6**, 429.
31 R. P. Megens and G. Roelfes, *Chem.–Eur. J.,* 2011, **17**, 8514.
32 Z. Tang, H. Iida, H.-Y. Hu and E. Yashima, *ACS Macro Lett.*, 2012, **1**, 261.
33 H. Iida, Z. Tang and E. Yashima, *J. Polym. Sci., Part A: Polym. Chem.*, 2013, **51**, 2869–2879.
34 E. Yashima, *Polymer Journal* 2010, **42**, 3.
35 R. Motoshige, Y. Mawatari, A. Motoshige, Y. Yoshida, T. Sasaki, H. Yoshimizu, T. Suzuki, T. Yoshiharu and M. Tabata, J. *Polym. Sci., Part A: Polym. Chem*., 2013, **52**, 752.
36 Y. Yoshida, Y. Mawatari, A. Motoshige, R. Motodshige, T. Hiraokib and M. Tabata, *Polym. Chem*., 2013, **4**, 2982.
37 Y. Yoshiaki, Y. Mawatari, A. Motoshige, R. Motoshige, T. Hiraoki, M. Wagner, K. Müllen and M. Tabata, *J. Am. Chem. Soc*., 2013, **135**, 4110.
38 K. K. L. Cheuk, J. W. Y. Lam, J. Chen, M. L. Lai and B. Z. Tang, *Macromolecules*, 2003, **36**, 5947.
39 B. S. Li, K. K. L. Cheuk, L. Ling, J. Chen, X. Xiao, C. Bai and B. Z. Tang, *Macromolecules*, 2003, **36**, 77.
40 J. W. Y. Lam and B. Z. Tang*, Acc. Chem. Res*., 2005, **38**, 745.
41 M. G. Mayershofer and O. J. Nuyken, *Polym. Sci. Part A: Polym. Chem.*, 2005, 43, 5723.
42 K. K. L. Cheuk, B. S. Li, J. W. Y. Lamand B. Z. Tang, *Macromolecules*, 2008, **41**, 5997.
43 L. Liu, T. Namikoshi, Y. Zang, T. Aoki, S. Hadano, Y. Abe, I. Wasuzu, T. Tsutsuba, M. Teraguchi and T. J. Kaneko*, J. Am. Chem. Soc.*, 2013, **135**, 602.
44 J. G. Rudick and V. Percec, *Macromol. Chem. Phys*., 2008, **209**, 1759.
45 M. Asahi, Y. Mawatari, R. Motoshige, Y. Yoshida and M. Tabata, *J. Polym. Sci., Part A: Polym. Chem.*, 2013, **51**, 5177.
46 X. -Q. Liu, J. Wang, Sh. Yang and E.-Q. Chen, *ACS Macro Lett*., 2014, **3**, 834.
47 J. Kumaki, S. -I. Sakurai and E. Yashima, *Chem. Soc. Rev.,* 2009, **38**, 737.
48 F. Freire, E. Quiñoá, R. Riguera, *Chem. Rev.*, 2016, **116**, 1242.
49 T. Nishimura, K. Takatani, S. Sakurai, K. Maeda and E. Yashima, Angew. Chem., Int. Ed., 2002, **41**, 3602.
50 S. -I. Sakurai, K. Kuroyanagi, K. Morino, M. Kunitake, E. Yashima, *Macromolecules* 2003, **36**, 9670.
51 S. -I. Sakurai, A. Ohira, Y. Suzuki, R. Fujito, T. Nishimura, M. Kunitake and E. Yashima, *J. Polym. Sci. Part A: Polym. Chem.,* 2004, **42**, 4621.
52 K. Okoshi, S. –I. Sakurai, J. K. Ohsawa, J. Kumaki and E. Yashima, Angew. Chem., Int. Ed., 2006, **45**, 8173.
53 S. –I. Sakurai, K. Okoshi, J. Kumaki and E. Yashima, Angew. Chem., Int. Ed., 2006, **45**, 1245.
54 S. -I. Sakurai, K. Okoshi, J. Kumaki and E. Yashima, *J. Am. Chem. Soc.*, 2006, **128**, 5650.
55 S. -I. Sakurai, K. Ohsawa, K. Nagai, K. Okoshi, J. Kumaki and E. Yashima, *Angew. Chem., Int. Ed*., 2007, **46**, 7605.
56 S. Ohsawa, S.-I. Sakurai, K. Nagai, M. Banno, K. Maeda, J. Kumaki and E. Yashima, *J. Am. Chem. Soc*., 2011, **133**, 108.
57 S. Ohsawa, S.-I. Sakurai, K. Nagai, K. Maeda, J. Kumaki, E. Yashima, *Polym. J.* 2012, **44**, 42.
58 F. Freire, J. M. Seco, E. Quiñoá, R. Riguera, *Angew. Chem., Int. Ed.* 2011, **50**, 11692.
59 Freire, J. M. Seco, E. Quiñoá, R. Riguera, *J. Am. Chem. Soc.* 2012, **134**, 19374.
60 S. Arias, F. Freire, E. Quiñoá, R. Riguera, *Angew. Chem., Int. Ed.* 2014, **53**, 13720
61 S. Arias, F. Freire, E. Quiñoá, R. Riguera, *Polym. Chem.* 2015, **6**, 4725.
62 S. Arias, J. Bergueiro, F. Freire, E. Quiñoá, R. Riguera, small 2016, **12**, 238.
63 I. Louzao, J. M. Seco, E. Quiñoá, R. Riguera, *Angew. Chem., Int. Ed.* 2010, **49**, 1430.
64 J. Bergueiro, F. Freire, E. P. Wendler, J. M. Seco, E. Quiñoá, R. Riguera, Chem. Sci. 2014, **5**, 2170
65 S. Leiras, F. Freire, J. M. Seco, E. Quiñoá, R. Riguera, *Chem. Sci.* 2013, **4**, 2735.
66 S. Leiras, F. Freire, E. Quiñoá, R. Riguera, *Chem. Sci.* 2015, **6**, 246.
67 Z. –Q. Wu, K. Nagai, M. Banno, K. Okoshi, K. Onitsuka, and E. Yashima, *J. Am. Chem. Soc.* 2009, **131**, 6708.
68 M. Banno, Z. –Q. Wu, K. Nagai, S.-I. Sakurai, K. Okoshi and E. Yashima, *Macromolecules* 2010, **43**, 6553.
69 T. Miyabe, H. Iida, M. Banno, T. Yamaguchi and E. Yashima, Macromolecules 2011, **44**, 8687.
70 M. Banno, T. Yamaguchi, K. Nagai, C. Kaiser, Stefan Hecht and Eiji Yashima *J. Am. Chem. Soc.*, 2012, **134**, 8718.
71 V. Percec, M. Obata, J. G. Rudick, B. B. De, M. Glodde, T. K. Bera, S. N. Magonov, V. S. K. Balagurusamy, P. A. Heiney, *J. Polym. Sci., Part A: Polym. Chem.* 2002, **40**, 3509.
72 V. Percec, J. G. Rudick, M. Peterca, S. R. Staley, M. Wagner, M. Obata, C. M. Mitchell, W.-D. Cho, V. S. K. Balagurusamy, J. N. Lowe, M. Glodde, O. Weichold, K. J. Chung, N. Ghionni, S. N. Magonov, P. A. Heiney, *Chem. - Eur. J.* 2006, **12**, 5731.
73 V. Percec, J. G. Rudick, M. Wagner, M. Obata, C. M. Mitchell, W.-D. Cho, S. N. Magonov, *Macromolecules* 2006, **39**, 7342.
74 G. G. Roberts, *Langmuir-Blodgett Films;* Plenum: New York, 1990.
75 T. Kawauchi, J. Kumaki, A. Kitaura, K. Okoshi, H. Kusanagi, K. Kobayashi, T. Sugai, H. Shinohara and E. Yashima, *Angew. Chem., Int. Ed.,* 2008, **47**, 515.
76 B. S. Li, J. W. Y. Lam, Z.-Q. Yu, B. Z. Tang, *Langmuir* 2012, **28**, 5770.
77 K. K. L. Cheuk, J. W. Y. Lam, Y. Xie, B. Z. Tang, *Macromolecules* 2008, **41**, 5997.
78 B. S. Li, S. Z. Kang, K. K. L. Cheuk, L. Wan, L. Ling, C. Bai, B. Z. Tang, *Langmuir* 2004, **20**, 7598.
79 B. S. Li, K. K. L. Cheuk, L. Ling, J. Chen, X. Xiao, C. Bai, B. Z. Tang, *Macromolecules* 2003, **36**, 77.
80 K. K. L. Cheuk, J. W. Y. Lam, L. M. Lai, Y. Dong, B. Z. Tang, *Macromolecules* 2003, **36**, 9752.
81 B. S. Li, K. K. L. Cheuk, F. Salhi, J. W. Y. Lam, J. A. K. Cha, X. Xiao, C. Bai, B. Z. Tang, *Nano Lett.* 2001, **1**, 323.
82 A. Ulman, An Introduction to Ultrathin, Organic Films—From Langmuir-Blodgett to Self-Assembly, Academic Press, New York, 1991.
83 R. Rodríguez, E. Quiñoá, R. Riguera, F. Freire *Nanoscale*, 2016, **8**, 3362.
84 S. Sakurai, K. Kuroyanagi, R. Nunokawa and E. Yashima, *J. Polym. Sci. Part A: Polym. Chem*., 2004, **42**, 5838.
85 S. Matsushita and K. Azagi*, J. Am. Chem. Soc*., 2015, **137**, 9077.
86 T. Mori, M. Kyotani and K. Azagi, *Chem. Sci.,* 2011, **2**, 1389.

87 K. Akagi, *Chem. Rev.*, 2011, **109**, 5354.
88 T. Mori, M. Kyotani and K. Azagi, *Macromolecules*, 2010, **43**, 8363.
89 B. S. Li, K. K. L. Cheuk, D. Yang, J. W. Y. Lam, L. J. Wan, C. Bai, B. Z. Tang, *Macromolecules* 2003, **36**, 5447.
90 K. Shinohara, S. Yasuda, G. Kato, M. Fujita, H. Shigekawa, *J. Am. Chem. Soc.* 2001, **123**, 3619.
91 R. Rodríguez, E. Quiñoá, R. Riguera, F. Freire, *J. Am. Chem. Soc.* 2016, **138**, 9620.

GA